Double bi-material cantilever structures for complex surface plasmon modulation

Eui-Young Song,[1] Jaebum Cho,[1] Hwi Kim,[2,*] Woo Young Choi,[3] and Byoungho Lee[1]

[1]*National Creative Research Center for Active Plasmonics Application Systems, Inter-University Semiconductor Research Center and School of Electrical Engineering, Seoul National University, Gwanak-gu Gwanakro 1, Seoul 151-774, South Korea*
[2]*Department of Electronics and Information Engineering, College of Science and Technology, Korea University, 2511 Sejong-ro, Sejong 339-700, South Korea*
[3]*Department of Electronic Engineering, Sogang University,35 Baekbeom-ro, Mapo-gu, Seoul 121-742, South Korea*
[*] *hwikim@korea.ac.kr*

Abstract: A complex modulation structure of surface plasmon polaritons using double bi-material cantilevers is proposed. It is shown with numerical analysis that the thermally controlled mechanical actuation of double bi-material cantilevers can modulate the amplitude and phase of surface plasmon polaritons across a full complex modulation range independently and simultaneously. The complex modulation structures designed for visible wavelengths are presented and their multi-wavelength integration is discussed.

OCIS codes: (240.6680) Surface plasmons; (250.5300) Photonic integrated circuits; (070.6120) Spatial light modulators .

References and links

1. H. Kim, C.-Y. Hwang, K.-S. Kim, J. Roh, W. Moon, S. Kim, B.-R. Lee, S. Oh, and J. Hahn, "Anamorphic optical transformation of an amplitude spatial light modulator to a complex spatial light modulator with square pixels [invited]," Appl. Opt. **53**(27), G139–G146 (2014).
2. S. Choi, J. Roh, H. Song, G. Sung, J. An, W. Seo, K. Won, J. Ungnapatanin, M. Jung, Y. Yoon, H.-S. Lee, C.-H. Oh, J. Hahn, and H. Kim, "Modulation efficiency of double-phase hologram complex light modulation macro-pixels," Opt. Express **22**(18), 21460–21470 (2014).
3. K. J. A. Ooi, P. Bai, S. C. Hong, and L. K. Ang, "Ultracompact vanadium dioxide dual-mode plasmonic waveguide electroabsorption modulator," Nanophotonics **2**(1), 13–19 (2013).
4. J. T. Kim, "CMOS-compatible hybrid plasmonic modulator based on vanadium dioxide insulator-metal phase transition," Opt. Lett. **39**(13), 3997–4000 (2014).
5. J. Gosciniak and S. I. Bozhevolnyi, "Performance of thermo-optics components based on dielectric loaded surface plasmon polariton waveguides," Sci. Rep. **3**, 1803 (2013).
6. J. Gosciniak and D. T. H. Tan, "Theoretical investigation of graphene-based photonic modulators," Sci Rep **3**, 1897 (2013).
7. W.-C. Chiu, C.-C. Chang, J.-M. Wu, M.-C. M. Lee, and J.-M. Shieh, "Optical phase modulators using deformable waveguides actuated by micro-electro-mechanical systems," Opt. Lett. **36**(7), 1089–1091 (2011).
8. S. Y. Zhu, G. Q. Lo, and D. L. Kwong, "Phase modulation in horizontal metal-insulator-silicon-insulator-metal plasmonic waveguides," Opt. Express **21**(7), 8320–8330 (2013).
9. J. Lloret, R. Kumar, S. Sales, F. Ramos, G. Morthier, P. Mechet, T. Spuesens, D. Van Thourhout, N. Olivier, J. M. Fédéli, and J. Capmany, "Ultra-compact electro-optic phase modulator based on III-V-on-Silicon microdisk resonator," Opt. Lett. **37**(12), 2379–2381 (2012).
10. L. Liao, D. Samara-Rubio, M. Morse, A. Liu, D. Hodge, D. Rubin, U. Keil, and T. Franck, "High speed silicon Mach-Zehnder modulator," Opt. Express **13**(8), 3129–3135 (2005).
11. W. M. Green, M. J. Rooks, L. Sekaric, and Y. A. Vlasov, "Ultra-compact, low RF power, 10 Gb/s silicon Mach-Zehnder modulator," Opt. Express **15**(25), 17106–17113 (2007).
12. L. Chen, K. Preston, S. Manipatruni, and M. Lipson, "Integrated GHz silicon photonic interconnect with micrometer-scale modulators and detectors," Opt. Express **17**(17), 15248–15256 (2009).
13. Q. Xu, B. Schmidt, S. Pradhan, and M. Lipson, "Micrometre-scale silicon electro-optic modulator," Nature **435**(7040), 325–327 (2005).
14. Q. Xu, S. Manipatruni, B. Schmidt, J. Shakya, and M. Lipson, "12.5 Gbit/s carrier-injection-based silicon micro-ring silicon modulators," Opt. Express **15**(2), 430–436 (2007).
15. D. Pacifici, H. J. Lezec, and H. A. Atwater, "All-optical modulation by plasmonic excitation of CdSe quantum dots," Nat. Photonics **1**(7), 402–406 (2007).

16. D. Feng, S. Liao, H. Liang, J. Fong, B. Bijlani, R. Shafiiha, B. J. Luff, Y. Luo, J. Cunningham, A. V. Krishnamoorthy, and M. Asghari, "High speed GeSi electro-absorption modulator at 1550 nm wavelength on SOI waveguide," Opt. Express **20**(20), 22224–22232 (2012).
17. E. Palik, *Handbook of Optical Constants of Solids* (Academic, 1985).
18. G. Vuye, S. Fisson, V. Nguyen Van, Y. Wang, J. Rivory, and F. Abeles, "Temperature dependence of the dielectric function of silicon using in situ spectroscopic ellipsometry," Thin Solid Films **233**(1-2), 166–170 (1993).
19. S. Rojebuathong, P. Chindaudom, W. Luangtip, M. Horphatum, P. Eiamchai, V. Patthanasetthakul, and P. Limsuwan, "Temperature dependence of optical constants of silver film studied by in situ spectroscopic ellipsometry," Advanced Materials Research **445**, 55–57 (2008).
20. W. Riethmuller and W. Benecke, "Thermally excited silicon microactuators," IEEE Trans. Electron. Dev. **35**(6), 758–763 (1988).
21. H. Conley, N. V. Lavrik, D. Prasai, and K. I. Bolotin, "Graphene bimetallic-like cantilevers: probing graphene/substrate interactions," Nano Lett. **11**(11), 4748–4752 (2011).

1. Introduction

The simultaneous modulation of both the amplitude and phase of optical waves, i.e., complex optical modulation, has been considered the ultimate modulation capability for the perfect control and manipulation of optical waves. In principle, the complex modulation of an optical field means the perfect generation of an arbitrary wave-front profile and such a capability would lead to the innovation of technologies in many fields of optical science and engineering such as digital holographic engineering, optical and quantum communication, and optical computing.

Although the superior properties of the complex modulator are well recognized, the complex modulator has not yet been realized in the form of a compact device structure. Bulky system level implementation of complex modulation have been actively investigated [1] and, recently, the micro-diffractive optic design of complex modulator were reported [2]. However, most present photonic modulations are amplitude-only [3–6] or phase-only [7–9] types. Although various photonic modulation mechanisms such as the classical Mach-Zehnder interferometer [10, 11], ring-resonator [12–14], and bandgap absorption [15, 16] have been developed, previous reports on principal mechanisms or integrated device structures for complex optical modulation have been very rare.

In this paper, a novel mechanism of surface plasmon polariton (SPP) mediated complex optical modulation is proposed. To accomplish the goal, we use a thermo-mechanical method of active complex optical modulation. The research on thermo-optical [3–5] and thermo-mechanical [7] manipulation of optical fields has been increasing recently. In the proposed design, a thermally controlled double bi-material structure is chosen as the active actuation structure. This paper is organized as follows. In section 2, the design and operating principle of the proposed thermo-mechanical optical complex modulation structure are described. In section 3, the complex modulation characteristics of the proposed structure are numerically analyzed. In section 4, the scale-down and multi-wavelength integration issues in a device application point of view are discussed and concluding remarks are given in section 5.

2. Thermo-mechanical complex modulation structure

Figure 1 schematically depicts the proposed thermo-mechanical complex optical modulation configuration. The structure is divided into two parts for (i) amplitude modulation and (ii) phase modulation. The former is composed of a silver/silicon bi-material cantilever, while the latter is a bi-material/free-space/metal waveguide structure. The thin bi-material made of silver and silicon can be bent toward the silicon side by raising the temperature due to the difference in thermal expansion coefficients. By default, at room temperature (T_0 = 25°C), the cantilevers of the amplitude and phase modulation parts are collinearly aligned along the x-axis as shown in Fig. 1(a).

Once the input SPP launched on the left bi-material cantilever reaches the narrow gap between the amplitude and phase modulation section, a part of the SPP crosses the gap and is transmitted to the phase modulation section which is a MIM (Metal-Insulator-Metal) plasmonic waveguide. The transmission ratio across the gap is highly dependent on the

#229169 - $15.00 USD Received 8 Dec 2014; revised 20 Jan 2015; accepted 6 Feb 2015; published 23 Feb 2015

vertical gap size on the y-axis. When the temperature of the bi-material cantilever in the amplitude modulation part, T_A, starts to rise over a threshold temperature, the bi-material cantilever begins to bend downward as shown in Fig. 1(b). This bending leads to a reduction of the SPP transmission ratio across the intermediate gap, facilitating the amplitude modulation. Interestingly, it can be shown that the gap causing amplitude modulation hardly affects the phase of SPP transmitted. The vertical gap variation on the y-axis, only influences the amplitude of the evanescent tail of the SPP, but the phase of the SPP at that point is conserved. The reason of this argument will be further explained in the later part.

Contrasting the bi-material cantilever in the amplitude modulation part, the one in the phase modulation part is designed to be bent upward with increasing temperature T_P as shown in Fig. 1(b). This bending action transforms the MIM plasmonic waveguide with a constant effective refractive index to a width-tailored MIM waveguide with a continuously varying effective refractive index profile along the x-axis. The degree of bend is controlled stably by the local temperature T_P, causing the phase delay through the phase modulation section to be of finite length. As a result, the dynamic phase modulation capability is achieved.

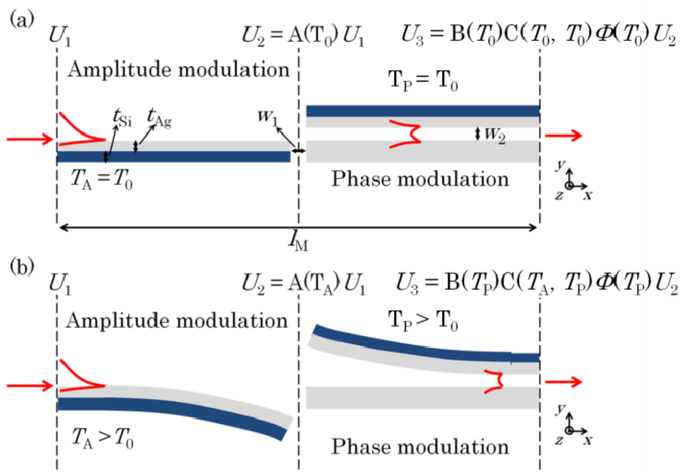

Fig. 1. Schematic diagram of complex modulation using bi-material cantilever. The situations for (a) $T_{A,\,P} = T_0$ and (b) $T_{A,\,P} > T_0$. The footprint length of the structure is denoted by l_M.

More specifically, for an input SPP U_1, the SPP signal at the center gap is represented by $A(T_A)U_1$ in which $A(T_A)$ is the amplitude modulation factor as a function of temperature T_A. The complex amplitude of the SPP at the output point is represented by $D(T_A,\ T_P) = A(T_A)B(T_P)C(T_A,T_P)\Phi(T_P)U_1$ in which $B(T_P)$ and $\Phi(T_P)$ are the amplitude and phase modulation coefficients, which are dependent on T_P. $B(T_P)$ indicates that the bending of the bi-material cantilever in the phase modulation part could affect the amplitude of the output signal. $C(T_A,T_P)$ is the coupling coefficient at the center gap, which reflects the dependence of the entrance width of the MIM waveguide on T_P. As the width of MIM plasmonic waveguide in the phase modulation part gets wider, the amount of SPP signal entering into the phase modulation MIM waveguide increases. The proposed structure provides a sufficient degree of freedom in the complex SP modulation with the thermal adjustment of cantilever bending.

3. Complex modulation characteristics of the proposed structure

The complex SPP modulation characteristics of the model structure shown in Fig. 1 is analyzed with the multi-physics numerical simulator, COMSOL Multiphysics (Ver 4.3). The structural parameters are set as follows: silver layer thickness t_{Ag} = 100 nm, silicon layer thickness t_{Si} = 100 nm, gap width w_1 = 60 nm, and the footprint of the modulator l_M = 16μm. The free space wavelength of the optical field is set to 650 nm. The thermo-optical parameters of silver and silicon related to bi-material action are extracted from literature [17–19].

The z-directional magnetic field distributions at selected temperatures are shown in Figs. 2(a)-2(e). At room temperature (T_A = 25 °C and T_P = 25°C), the cantilevers of the amplitude and phase modulation parts have no bend and are exactly parallel to the x-axis as shown in Fig. 2(a). In this case, the amplitude modulation is estimated to be 0.375. As T_P rises, the bi-material cantilever in the phase modulation part bends upward (Fig. 2(b)) varying the effective axial refractive index profile of the resultant width-tapered MIM waveguide. This causes a phase change in the output SPP wave at the end of the phase modulation section. In the simulation, a phase changes of π and 1.5π were achieved by temperature changes from T_P = 25 °C to T_P = 90 °C and from T_P = 25 °C to T_P = 130 °C, respectively (Figs. 2(b) and Figs. 2(d)). Also, the propagation loss of SPP is dependent on the temperature. Therefore, not only the phase but also the amplitude of the output SPP signal are varied with T_P. For that reason, in the case of Fig. 2(b), the amplitude modulation is estimated to be 0.6 twice as big as that of the case of Fig. 2(a). When T_P is room temperature and T_A is higher than room temperature, only the bi-material cantilever in the amplitude modulation part bends downward as shown in Fig. 2(c). Since the thermal expansion causes a higher deflection of the bi-material cantilever along the y-axis Δy (0 nm ~400 nm between 25 °C and 400 °C) than increase in the cantilever's length Δl (0 nm ~15 nm between 25 °C and 400 °C), we can make the simplifying approximation that the variation in the gap along the y-axis with T_A is just due to the former deflection. The cantilever bend in the amplitude modulation section increases both the scattering in the widened gap and the scattering element on the curved surface of the bi-material cantilever. In the case of Fig. 2(c), the amplitude modulation is estimated to be about 0.25 which is lower than 0.3, that of Fig. 2(a). When both T_A and T_P are set higher than room temperature, as shown in Fig. 2(d), both the gap width affected by T_A and the entrance width of the phase section MIM affected by T_P are widen. The amplitude and phase modulations of the output SPP signal are affected by several factors such as additional radiation on the curved cantilever surface, propagation loss, magnified scattering in the shape modification with the widened intermediate gap and entrance of the phase part MIM waveguide. The dependency of the complex modulation of the output SPP on T_A and T_P is strengthened. T_A can be increased to the degree sufficient to extinct the output signal as presented in Fig. 2(e). At T_A = 190 °C and T_P = 25 °C, the amplitude modulation is down to 0.04. It is noteworthy that the modulation extinction ratio can reach zero at an extremely high temperature of T_A, because the thermal loss becomes extremely high in the cantilever at that temperature. The complex modulation values in Figs. 2(a)-2(e) are indicated in the complex plane of Fig. 2(f).

The full dynamic range of the complex modulation is analyzed in terms of the temperature pair T_A and T_P. In Figs. 3(a) and 3(b), the amplitude and phase modulations, respectively, are plotted with respect to the temperature pair. It is of note that the amplitude modulation is seen as a nonlinear function not only of T_A but also of T_P. This relation can be explained by the competition between the thermal propagation loss and the transmission ratio into the MIM waveguide. An increase in T_P causes a higher transmission ratio at the gap and a higher thermal loss at the MIM waveguide simultaneously. Thus in Fig. 3(a) two regions can be observed separated by a critical value of T_P (130 °C); (i) a width dominant region at a relatively low temperature and (ii) a loss dominant region at a relatively high temperature. While in the region corresponding to T_P below 130 °C, the amplitude modulation tends to increase with T_P in the region corresponding to T_P above 130°C it tends to decrease.

In Fig. 3(a), white solid lines are contour lines representing the amplitude modulation of 0.2, 0.24, 0.3, and 0.375, respectively. On the other hand, in Fig. 3(b), the white contour lines represent a 0~2π phase modulation range. Overall, this proposed complex modulator can have a 0~2π phase modulation range below a 0.375 amplitude modulation.

#229169 - $15.00 USD Received 8 Dec 2014; revised 20 Jan 2015; accepted 6 Feb 2015; published 23 Feb 2015

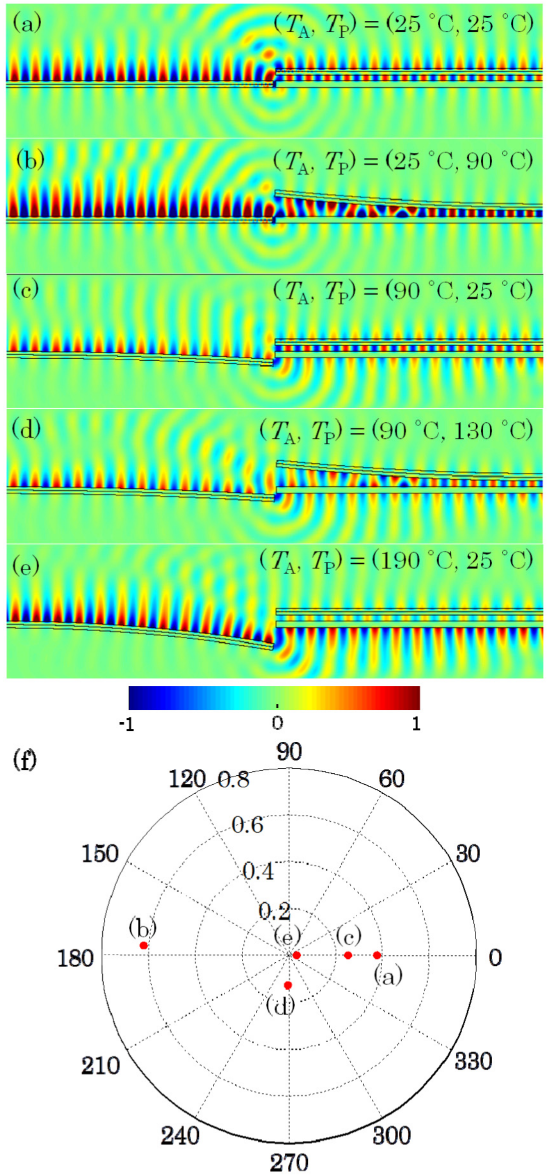

Fig. 2. *z*-directional magnetic field distribution (a.u.), H_z, at the selected temperatures (T_A, T_P) = (a) (25 °C, 25 °C), (b) (25 °C, 90 °C), (c) (90 °C, 25°C), (d) (90 °C, 130 °C), and (e) (190 °C, 25 °C), respectively. (f) Amplitude and phase modulation values of the output signals in the cases of Figs. 2(a)-2(e).

Actually, to independently and simultaneously modulate the amplitude and phase of surface plasmon wave, we have to choose appropriate control temperature pair (T_A,T_P). The trace (or table) of the control temperature pair analyzed in Fig. 3 can be used to choose proper control temperatures for a specific complex modulation. In general, if we want phase modulation to be P and the amplitude modulation to be A, we have to firstly draw the equi-amplitude equi-phase contours in the T_A-T_P space as presented in Figs. 3(a) and 3(b), and try to find the intersection point of two contours. At that point, we can obtain the control temperature pair for the specific complex modulation.

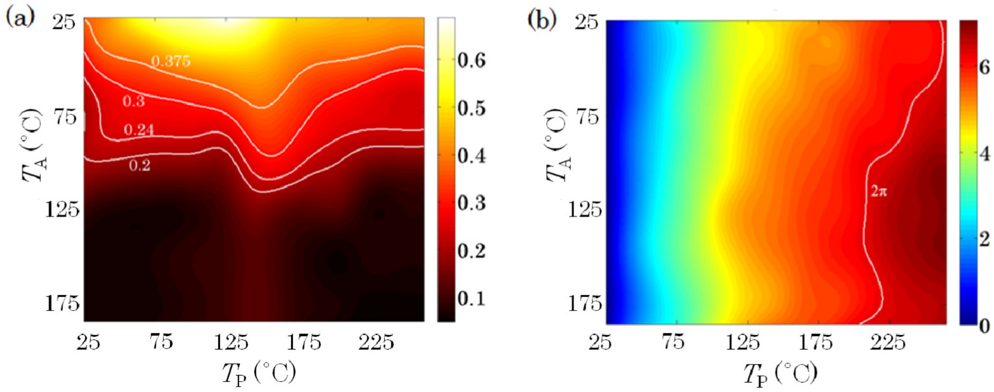

Fig. 3. Full dynamic range of complex modulation: (a) amplitude and (b) phase modulations of the output SPP signal.

4. Discussion about scaling-down and multi-wavelength integration

The structure scale-down is an important issue. From the point of view of device architecture, a small footprint length l_M (Fig. 1) is preferable. In Fig. 4, the amplitude modulation profiles for amplitude section cantilevers of lengths 4 μm, 8 μm, 12 μm, and 16 μm are analyzed with T_A varying from 25 to 300 °C for operating wavelength of 650nm. In this analysis, the other geometrical parameters are kept constant with the previous studies except that the bi-material cantilever of the phase modulation region is removed for simplicity. In Fig. 4, the amplitude modulation depths for the cases l_M = 4 μm, 8 μm, 12 μm, and 16 μm are analyzed to be 32.2%, 73.3%, 88.7%, and 94.4%, respectively. It is clear that longer cantilevers have a greater modulation depth, although more optical energy is lost through SPP propagation loss.

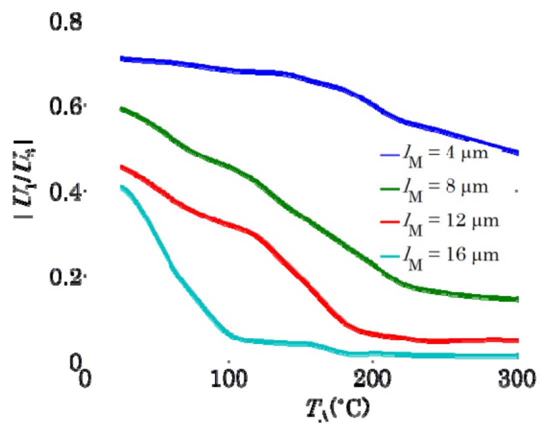

Fig. 4. Amplitude modulation under temperature ranging from 25 to 300°C with l_M of 4 μm, 8 μm, 12 μm, and 16 μm. The free space wave is set to 650 nm.

To develop the proposed cantilever modulator structure for its application as a visible-band multi-wavelength complex optical modulator, we need to design an integrated system of complex modulation structures for red (650nm), green (550nm), and blue (450nm) wavelengths. Interestingly, it can be inferred from the data in Fig. 4 that the footprints of modulators will lengthen with operating wavelength because the SPP evanescent tail will be elongated at longer wavelengths. At longer operating SPP wavelengths, a longer deflection length Δl may be required to invoke similar amplitude modulations to those available when the SPP operation wavelength is shorter.

#229169 - $15.00 USD Received 8 Dec 2014; revised 20 Jan 2015; accepted 6 Feb 2015; published 23 Feb 2015

For the integration of red, green, and blue modulators, it is essential to tune the modulation structures optimally so that each has a similar amplitude modulation profile within the shared temperature control range of T_A and T_P. The analysis of the design result shown in Fig. 5 depicts the complex modulation profiles of differing total device lengths l_M selected for different wavelengths and indicates that the resultant output signals at all wavelengths can be effectively integrated. To obtain the full-360 phase modulation and reasonable amplitude modulation range greater than 10%, we designed the appropriate structure for each wavelength. In practice, the fabrication of bi-material complex modulator structures and the control of temperature can be implemented through M/NEMS technology, of which thermal actuator or sensor applications using bi-materials are good examples. Riethmuller et al. implemented silicon-metal sandwich microactuators using the MEMS process [20]. Conley et al. demonstrated silicon nitride-graphene sandwich cantilever beams for the investigation of the graphene/substrate interaction [21]. Graphene is now considered as a promising material for those objectives due to its high thermal capacitance. Also, in order to alleviate thermal transfer between the two sections, the structure needs to be placed in vacuum. Nowadays, hermetic sealing process is widely used for MEMS technology. If this hermetic sealing process is introduced, our proposed structure will be placed in vacuum and reasonable thermal isolation can be achieved.

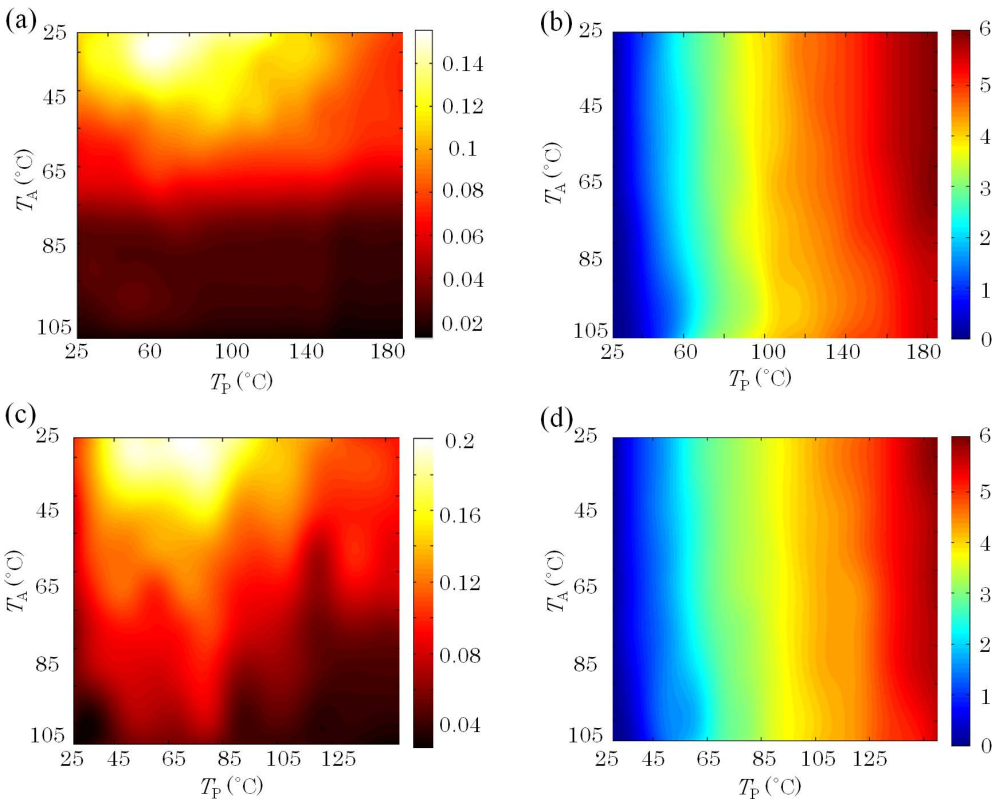

Fig. 5. Full dynamic range of complex modulation: (a) amplitude and (b) phase modulations for green wavelength (550nm) and (c)-(d) those for blue wavelength (450nm)

5. Conclusion

In conclusion, a design of a thermal bi-material cantilever based surface plasmon complex modulation structure has been proposed and its complex modulation characteristics and practical device issues relating to scale-down and multi-wavelength integration have been discussed. The proposed complex modulator has been shown to have such a relatively small

#229169 - $15.00 USD Received 8 Dec 2014; revised 20 Jan 2015; accepted 6 Feb 2015; published 23 Feb 2015

footprint that it would be fit for the integration of the red, green, and blue complex modulation structures which can potentially lead to the development of full-color complex spatial light modulator.

Acknowledgment

This work was supported by the National Research Foundation of Korea (NRF) grant funded by the Korea government (MSIP) (No. 2007-0054847).